

# Transmission and Reflection Spectra of a Photonic Crystal with a Raman Defects

V. G. Arkhipkin\* and S. A. Myslivets\*\*

*Kirenskii Institute of Physics, Siberian Branch, Russian Academy of Sciences, Krasnoyarsk, 660036 Russia  
Siberian Federal University, Krasnoyarsk, 660041 Russia*

\* e-mail: avg@iph.krasn.ru

\*\* e-mail: sam@iph.krasn.ru

Received March 15, 2010

**Abstract**—Features of Raman gain of probe radiation in three-level atoms placed in a defect of a one-dimensional photonic crystal in the presence of laser radiation (pump) at an adjacent high-frequency transition have been theoretically investigated. It has been shown that there is a pump intensity range where narrow peaks (resonances) simultaneously appear in the transmission and reflection spectra of the probe field. Beyond this region, the peak in the transmission spectrum is transformed to a narrow dip. The spectral position of these peaks is determined by the Raman resonance and the transmittance and reflectance can be larger than unity at pump intensities from several microwatts per square centimeter to several tens of milliwatts per square centimeter. The nature of narrow peaks is due to a sharp dispersion of a nonlinear refractive index near the Raman resonance; this dispersion is responsible for a strong decrease in the group velocity of probe radiation. The proposed scheme makes it possible to obtain controlled ultranarrow resonances in the transmission and reflection spectra of the photonic crystal.

**DOI:** 10.1134/S1063776110120022

## 1. INTRODUCTION

Photonic crystals have been actively investigated for two decades (see, e.g. [1, 2]). They have the unique combination of the dispersion properties and localization of radiation and, thus, make it possible to efficiently control light fluxes. Micro- and nanodefects in photonic crystals can localize light in a volume smaller than  $\lambda^3$  (where  $\lambda$  is the wavelength) with a high quality factor of defect modes (see [3, 4] and references therein). Such structures are often called photonic crystal cavities or micro- and nanocavities [5]. The photonic crystal cavities have important applications in various fields such as photonics [6], nonlinear optics [3], and quantum electrodynamics [7]. They underlie the developments of low-threshold microlasers [8], Raman lasers [9, 10], and devices for obtaining slow light and optically controlled delay lines [11]. A combination of a high quality factor of a microcavity and a small volume of a mode allowed the creation of Raman lasers with an ultralow lasing threshold (lower than 100  $\mu\text{W}$ ) [12, 13].

The presence of resonance media, e.g., atoms or quantum wells in a defect strongly modifies the spectral properties of the photonic crystal [14–17]. The use of electromagnetically induced transparency (EIT) [18] opens new unique opportunities to control the spectral properties of the photonic crystal [19] and to miniaturize optical filters, highly sensitive sensors, and completely optical switches and quantum mem-

ory. It was recently shown that the width of the transmission spectrum for the probe radiation in the photonic crystal with the defect containing an EIT medium can be reduced by a factor of about  $c/v_g \gg 1$  ( $c$  is the speed of light in vacuum and  $v_g$  is the group velocity of the probe wave in the EIT medium) due to a significant decrease in the group velocity under the EIT conditions and the quality factor of the defect mode increases correspondingly [20, 21].

The group velocity can also decrease under the Raman interaction of the probe (Stokes) radiation with the intense pump wave [22–25]; this decrease occurs with lower losses and in a wider spectral range than in the case of EIT [22]. We emphasize that the requirements to the choice of a medium in this case are less stringent than those for the case of EIT. In this work, the Raman interaction between two laser waves in a one-dimensional photonic crystal with the defect containing three-level atoms is theoretically studied. A new method is proposed to obtain controlled ultranarrow resonances in the transmission and reflection spectra of photonic crystals. The method is based on the effect of a decrease in the group velocity of the probe radiation in the presence of the Raman gain in the defect layer of a photonic crystal. The power of pump radiation is chosen below the threshold of stimulated Raman scattering (SRS), but above a value ensuring a noticeable enhancement of the probe wave. In contrast to spontaneous RS, the phasing of atomic vibrations occurs in this case in the volume occupied

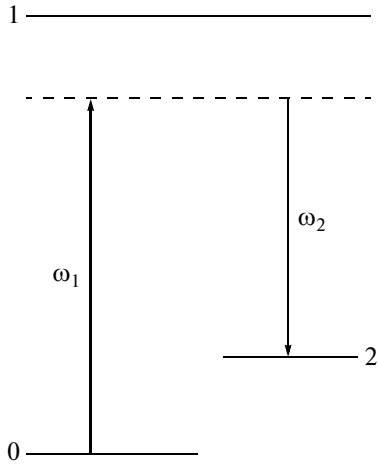


**Fig. 1.** Energy diagram of the three-level atom in the Raman gain scheme;  $\omega_1$  and  $\omega_2$  are the pump and probe frequencies, respectively; and 0 and 2 are the ground and metastable states, respectively.

by light waves as in the case of SRS, but uncontrolled instabilities do not appear. This scheme is low sensitive to fluctuations of the pump intensity [26] and the spectral resolution is determined by the spectrum width of the used laser beams and can, in principle, be high. The proposed method can be used in high-resolution Raman spectroscopy of gases and liquids [26], as well as for the creation of high-efficiency Raman amplifiers [27, 28].

## 2. MODEL AND APPROXIMATIONS

### 2.1. Nonlinear Raman Susceptibility and Group Velocity

The Raman gain of the probe wave with frequency  $\omega_2$  interacting with the pump wave with frequency  $\omega_1$  appears when the frequency difference  $\omega_1 - \omega_2$  is close to the frequency of an atomic or molecular transition  $\omega_{20}$ , i.e.,  $\omega_{20} \approx \omega_1 - \omega_2$  (see Fig. 1). It is due to the inelastic scattering of light [29]. This method is also called SRS enhancement [26]. The macroscopic explanation of the Raman gain is the Raman resonance of the cubic (Raman) susceptibility  $\chi_R(\omega_2, -\omega_1, \omega_1)$ . For three-level atoms with the energy levels shown in Fig. 1, a formula for the susceptibility  $\chi_R$  can be obtained by solving the equations for the density matrix in the third order of perturbation theory under the conditions

$$\begin{aligned} |\Omega_1| &= |\omega_{10} - \omega_1| \gg |G_1|, |G_2|, \gamma_{10}, \\ |G_1| &\gg |G_2|, \end{aligned}$$

where  $\Omega_1$  is the detuning from the one-photon resonance;  $\omega_{10}$  and  $\gamma_{10}$  are the resonance frequency and half-width of the  $|0\rangle - |1\rangle$  transition;  $2G_1 = d_{10}E_1/\hbar$  and  $2G_2 = d_{12}E_2/\hbar$  are the Rabi frequencies of the pump and probe waves, respectively; and  $E_1$  and  $E_2$  are the complex amplitudes of the pump and probe waves,

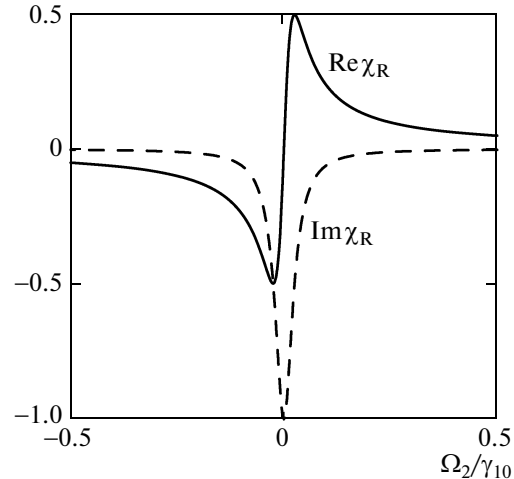


**Fig. 2.** Normalized (solid curve) real and (dashed curve) imaginary parts of the Raman susceptibility versus the detuning of the probe field.

respectively. Under these conditions, the population of the lower state  $|0\rangle$  can be treated as unchanged and the pump field, as given; i.e., quantity  $G_1$  is constant throughout the length of the medium.

In the given approximations, the Raman susceptibility for atoms at rest is given by the expression [30]

$$\chi_R(\omega_2) = \frac{1}{4\hbar^3 \Omega_1^2 (\Omega_2 + i\gamma_{20})} \frac{d_{21}^2 d_{10}^2}{d_{10}^2 + d_{12}^2}. \quad (1)$$

Here,  $\Omega_2 = \omega_{20} - (\omega_1 - \omega_2)$  is the detuning from the  $|0\rangle - |2\rangle$  Raman transition,  $\gamma_{20}$  is its half-width, and  $d_{ij}$  is the matrix dipole moment of the transition.

The real and imaginary parts of the susceptibility  $\chi_R = \chi'_R + i\chi''_R$  are shown in Fig. 2 as functions of the probe frequency. It is substantial that the imaginary part of  $\chi_R$  is negative near the Raman resonance; i.e., the probe wave is enhanced due to the transfer of the energy from the pump radiation to the probe field. In contrast to the one-photon resonance, the real part of  $\chi_R$  has the normal dispersion ( $\chi'_R/d\omega_2 > 0$ ).

For rarefied media, the complex refractive index  $n_2$  for the probe field under the Raman gain conditions is calculated by the standard method [31]

$$\begin{aligned} n_2(\omega_2) &= n'_2 + i n''_2 \\ &= \sqrt{1 + 4\pi N(\chi_2^{(1)} + \chi_R |E_1|^2)} \\ &\approx n_0(\omega_2) + 2\pi N\chi_R(\omega_2)|E_1|^2, \end{aligned} \quad (2)$$

where  $\chi_2^{(1)}$  and  $n_0 = 1 + 2\pi N\chi_2^{(1)}$  is the linear (nonresonance) susceptibility and the linear refractive index for the probe wave, respectively, and  $N$  is the density of atoms. The second term in Eq. (2) is the nonlinear part of the refractive index due to the Raman susceptibility.

Note that in the considered approximation,  $|\text{Im}\chi_R| \gg |\text{Im}\chi_2^{(1)}|$  and  $|\text{Re}\chi_2^{(1)}|$  leads only to the shift of the resonance frequency of the defect mode. For this reason, the contribution of  $\chi_2^{(1)}$  to the refractive index  $n_2$  will be neglected below.

According to the definition [32], the group velocity of the probe wave is

$$\begin{aligned} v_g &= \frac{c}{n'_2 + \omega_2(dn'_2/d\omega_2)} \\ &\approx \frac{c}{1 + 2\pi N|E_1|^2\omega_2(d\chi'_R/d\omega_2)} = \frac{c}{N_g}. \end{aligned} \quad (3)$$

Here,

$$N_g = 1 + 2\pi N|E_1|^2\omega_2 \frac{\partial\chi'_R}{\partial\omega_2} = 1 + \frac{K_{12}|G_1|^2}{\Omega_1^2\gamma_{20}^2}, \quad (4)$$

is the index of the group velocity, where  $K_{12} = 2\pi N\omega_2|d_{12}|^2/\hbar$ . The frequency derivative is taken at the point  $\omega_1 - \omega_2 = \omega_{20}$ . For simplicity, the dispersion of the linear nonresonance susceptibility is disregarded in Eq. (3) ( $n_0 \approx 1$ ).

Under the easily achieved condition  $K_{12}|G_1|^2/\Omega_1^2\gamma_{20}^2 \gg 1$ , the group velocity is given by the formula

$$v_g = c \frac{\Omega_1^2\gamma_{20}^2}{K_{12}|G_1|^2} \ll c. \quad (5)$$

According to Eq. (5), in contrast to the case of EIT [18], the group velocity is inverse proportional to the intensity of the control radiation, but the probe field is enhanced in this case. It is also noteworthy that  $v_g$  is proportional to the width of the Raman transition and is inverse proportional to the density of the medium. It is possible to control the group velocity of the probe radiation by varying the density of atoms and the intensity of the pump field. We emphasize that  $v_g$  decreases with a decrease in the width of the Raman transition. It can be shown that the group velocity in media where the EIT is observed can be  $10^{-9}$ – $10^{-6}c$ , i.e., the same as in the case of EIT.

## 2.2. Photonic Crystal with the Raman Defect

Let us consider a one-dimensional photonic crystal with the structure  $(\text{HL})^M\text{HDH}(\text{LH})^M$ . Here, H and L mark the dielectric layers with the high,  $n_H$ , and low,  $n_L$ , refractive indices, respectively; and with the thicknesses  $t_H$  and  $t_L$ , respectively; D is the defect layer with the refractive index  $n_D$  and thickness  $t_D$ ; and  $M$  is the number of periods. The defect layer is filled with a medium, which is modeled by three-level atoms at rest whose energy levels are shown in Fig. 1. The density of atoms is low enough to neglect the interaction between

them. The parameters of the photonic crystal are chosen such that the spectral width of excited defect modes is much larger than the widths of allowed transitions and  $|0\rangle - |2\rangle$  Raman transition (in contrast to [9, 10]).

Two plane monochromatic waves with frequencies  $\omega_1$  and  $\omega_2$  ( $\omega_1 > \omega_2$ ) are incident normally on the photonic crystal and propagate along the  $z$  axis, which is perpendicular to the photonic crystal layers ( $z = 0$  corresponds to the boundary of the first layer). The waves with frequencies  $\omega_1$  and  $\omega_2$  are called the pump or control wave and the probe or Stokes wave, respectively. The pump field  $E_1$  interacts with the  $|0\rangle - |1\rangle$  transition and the probe field  $E_2$  interacts with the adjacent  $|1\rangle - |2\rangle$  transition. The frequency difference  $\omega_1 - \omega_2$  is close to the Raman resonance frequency  $\omega_{20}$  of the dipole forbidden transition. Only the ground state  $|0\rangle$  is initially occupied. Note that the refractive index of the defect layer  $n'_2 = R n_2$  for the probe wave depends on the spatial coordinate  $z$ , because the field distribution in the defect is nonuniform because of the localization effect. For simplicity, we assume that the photonic crystal is in a medium with unity refractive index.

## 3. CALCULATION RESULTS AND THEIR ANALYSIS

### 3.1. Transmission and Reflection Spectra

The transmittance and reflectance were determined from the solution of the wave equations for the control and probe fields. In the stationary case, the field in an arbitrary  $j$ th layer can be represented as a superposition of the fields of counterpropagating waves,

$$E_j = A_j \exp[ik_j(z - z_j)] + B_j \exp[-ik_j(z - z_j)]. \quad (6)$$

Here,  $A_j$  and  $B_j$  are the amplitudes of the direct (incident) and inverse (reflected) waves, respectively, and  $k_j = n_j\omega_{1,2}/c$ , where  $n_j$  is the refractive index in the  $j$ th layer.

To obtain the amplitudes  $A_j$  and  $B_j$  in each layer, we used the recurrence relation method [21, 33] taking into account matching at the boundary of adjacent layers. The transmission and reflection spectra of the probe wave were determined by the formulas

$$T(\omega) = \frac{|A_2(L)|^2}{|A_{02}|^2}, \quad R(\omega) = \frac{|B_2(0)|^2}{|A_{02}|^2},$$

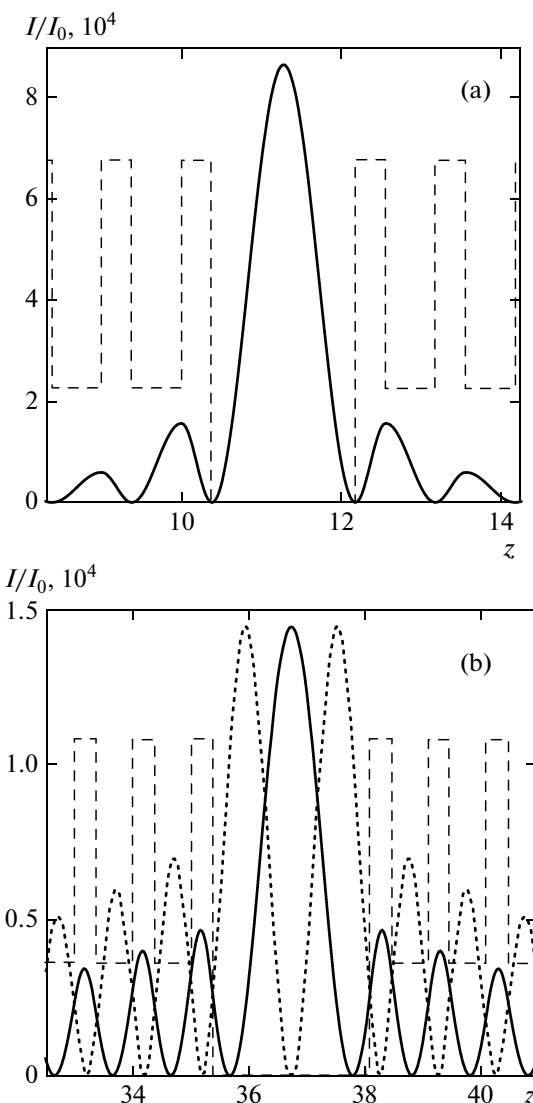
where  $A_{02}$  and  $A_2(L)$  are the amplitudes of the probe waves at the input ( $z = 0$ ) and output ( $z = L$ ) of the photonic crystal, respectively, and  $B_2(0)$  is the amplitude of the probe wave reflected from the input face ( $z = 0$ ).

The numerical simulation was performed for two cases. In the first case, the frequencies of the probe and control fields are close to each other and are both in one defect mode; i.e., the resonance frequency  $\omega_{20}$  is smaller than the spectral width of the defect mode. In the second case, the Raman transition frequency exceeds the width of the defect mode and, correspondingly, it is necessary to use two defect modes with the frequency difference close to the Raman transition frequency; this is the case of two interacting modes. The spatial distributions of these modes are different and this fact influences the magnitude of the effect under consideration.

Let us discuss the first case. For the numerical simulation of the transmission and reflection spectra, the parameters of the Raman medium were taken close to the parameters of sodium atoms. The wavelengths of the probe and pump fields were taken near the  $D$ -lines and  $\omega_{20}/2\pi = 1.8$  GHz. The parameters of the photonic crystal were  $M = 10$ ,  $n_H d_H = n_L d_L = \lambda_2/4$ ,  $d_D n_D = \lambda_2/2$ ,  $n_H = 2.35$ , and  $n_L = 1.45$ . The probe and control waves are in the transmission band of the photonic crystal, and the wavelength of the probe radiation  $\lambda_2$  was chosen such that its frequency under the Raman resonance condition ( $\omega_1 - \omega_2 = \omega_{20}$ ) coincides with the resonance frequency of the defect mode ( $\omega_0 = \omega_2$ ) at the detuning of the pump frequency  $\Omega_1 = 30\gamma_{10}$ ,  $\gamma_{10}/2\pi = 100$  MHz, and  $N \approx 10^{12} \text{ cm}^{-3}$ . The calculation of the field distribution in the defect with the chosen parameters indicates that the pump and probe waves almost completely overlap in space ( $n_D = 1$ ) (see Fig. 3a). As compared to the input values, the field intensity in the defect layer is increased by about five orders of magnitude due to the localization effect. It is assumed that  $|G_1| \gg |G_2|$  in the defect layer; for this reason, the field distribution inside the defect is treated as given when calculating the transmittance and reflectance for the probe fields.

The transmission and reflection spectra were calculated for various Rabi frequencies of the control field and various half-widths of the Raman transition  $\gamma_{20}$ . Figure 4 shows the typical transmission and reflection spectra of the photonic crystal for the probe wave under the Raman gain conditions when  $\gamma_{20} < \gamma_{10}$  (the width of the Raman transition is small). A narrow structure (a sharp peak or resonance), which is due to the Raman resonance, is seen in the center of the spectrum in Fig. 4a against the background of the wide transmission line corresponding to the empty defect ( $n_D = 1$  for both waves). In this case, the transmittance can be larger than unity. A narrow peak whose height can be larger than unity is also seen in the center of the dip in the reflection spectrum in Fig. 4b.

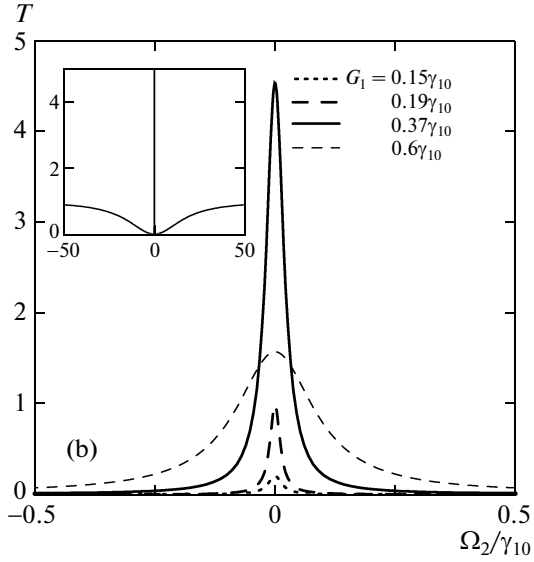
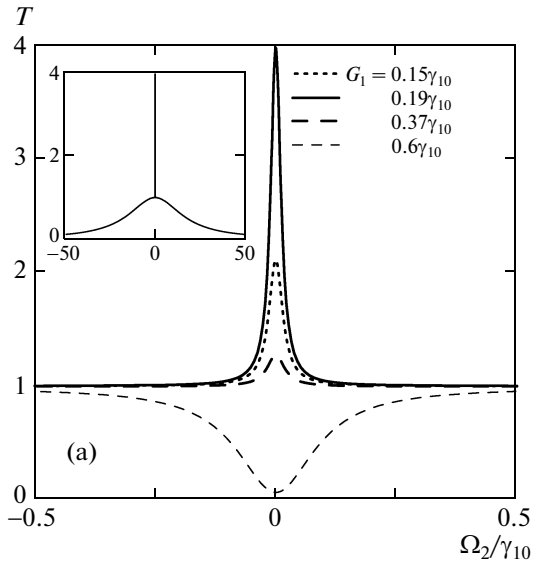
Figure 5 shows similar spectra at  $\gamma_{20} > \gamma_{10}$  (the wide Raman transition). In this case, the transmission and reflection spectra are much wider. Thus, the width of the transmission and reflection spectra decreases with



**Fig. 3.** Intensity distributions of the (solid curve) probe and (dotted curve) control fields in the region of the defect layer for the cases where (a) the frequencies of both fields are close to each other,  $M = 10$ , and  $d_D n_D = \lambda_2/2$  and (b) the difference between the frequencies of the fields is much larger than the width of the defect mode,  $M = 35$ , and  $d_D n_D = 3\lambda_2/4$ ; such a structure has two defect modes. The dashed lines schematically show the refractive index of the photonic crystal.

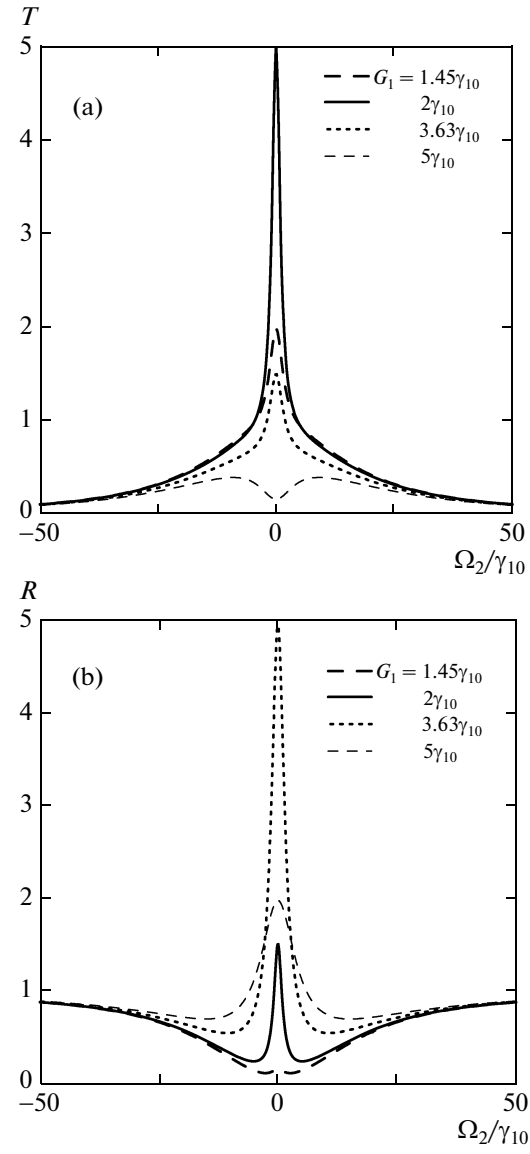
a decrease in the width of the Raman transition. The transmittance and reflectance depend both on the width of the Raman resonance and on the pump field intensity (see Fig. 6). It is interesting that the widths of the resonances  $\delta\omega$  can be smaller than the width of the Raman transition, as is seen in the insets in Fig. 6, where  $\delta\omega = \gamma_{20}/5$  for the parameters indicated in the figure.

Figure 7 shows the transmittance and reflectance as functions of the normalized Rabi frequency of the pump field for various widths of the Raman transition. As the pump intensity increases to a certain (thresh-



**Fig. 4.** (a) Transmission and (b) reflection spectra of the photonic crystal for various intensities of the control field for the case shown in Fig. 3a for  $\gamma_{10}/\gamma_{20} = 20$ . The insets show the spectra in a wider spectral range.

old) value, the transmittance and reflectance at the resonance frequency increase. Above this threshold, these quantities decrease. In this case, the peak in the transmission spectrum changes to a dip (see Fig. 4a) whose depth tends to zero with an increase in the control field. Another tendency is observed in the reflection spectrum: the reflectance tends to unity at sufficiently high control fields. The transmission and reflection are inverted in the center of the contour. When  $\gamma_{20} > \gamma_{10}$ , the behavior of the transmission and reflection spectra is qualitatively the same, but the spectra are much wider (see Fig. 5). As is seen in Fig. 7, there is a pump intensity range where the transmittance and reflectance are simultaneously larger than unity; as the ratio  $\gamma_{20}/\gamma_{10}$  increases, this range is expanded and larger pump intensities are required.



**Fig. 5.** Same as in Fig. 4, but for  $\gamma_{10}/\gamma_{20} = 0.2$ .

Let us consider the case of two modes where the frequency difference  $\omega_1 - \omega_2$  between the control and probe fields exceeds the spectral width of the defect mode. In this case, the parameters of the photonic crystal are chosen such that there are two defect modes with the frequency difference close to the frequency of the Raman transition (two-mode regime). Figure 3b shows the spatial distribution of the modes for the chosen configuration photonic crystal having two modes. The pump and probe waves excite modes near the short- and long-wavelength edges of the band gap, respectively. Figure 8 shows the transmission and reflection spectra of the probe wave in the two-mode regime for a hypothetical medium. It is seen that narrow resonances in the transmission and reflection

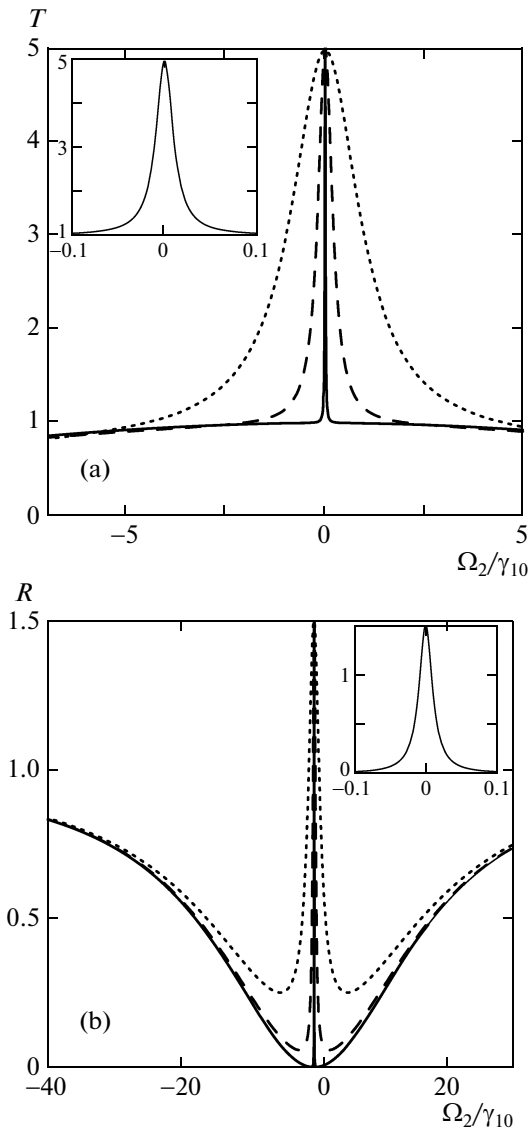


**Fig. 6.** (a) Transmission and (b) reflection spectra for various widths of the Raman transition  $\gamma_{20}$ :  $\gamma_{20}/\gamma_{10} =$  (solid curves) 0.05, (dashed curves) 1, and (dotted curves) 5 and various Rabi frequency of pump radiation  $G_1$ :  $G_1/\gamma_{10} =$  (solid curves) 0.2, (dashed curves) 0.895, and (dotted curves) 2.

spectra also exist in this case, but somewhat higher intensities of the control field are required. We explain this fact by the incomplete spatial overlapping of interacting modes.

Thus, peaks are simultaneously observed in the transmission and reflection spectra of the photonic crystal with the Raman enhancing defect. The heights and spectral positions of these peaks can be controlled by varying the amplitude and frequency of the control field. If the width of the Raman transition is small,  $\gamma_{20} \ll \gamma_{10}$ , ultranarrow resonances can be obtained in the transmission and reflection spectra.

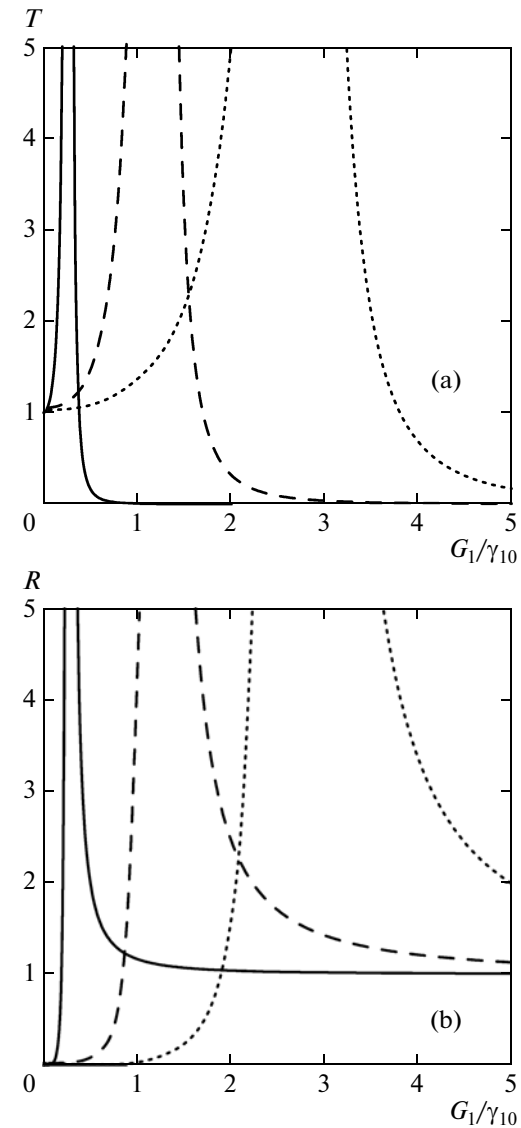


**Fig. 7.** Maximum (a) transmittance and (b) reflectance at the resonance frequency versus the normalized Rabi frequency of the pump field for  $\gamma_{20}/\gamma_{10} =$  (solid curves) 0.05, (dashed curves) 1, and (dotted curves) 5.

### 3.2. Discussion of the Results

The features of the behavior of the transmission and reflection spectra for the probe field can be qualitatively explained by using analogy with the Fabry–Perot cavity [4] that has length  $d$  equal to the thickness of the defect layer  $t_D$  and is filled with the Raman medium. The transmittance of the Fabry–Perot cavity for the probe wave,  $T = I_{2t}/I_{20}$  ( $I_{20}$  and  $I_{2t}$  are the intensities of light at the input of the Fabry–Perot cavity and passed light, respectively), in the presence of the pump wave can be calculated in the standard way [34]

$$T = \frac{T_M^2 e^{\alpha d}}{(1 - R_M e^{\alpha d})^2 + 4 R_M e^{\alpha d} \sin^2(\Phi/2)}.$$

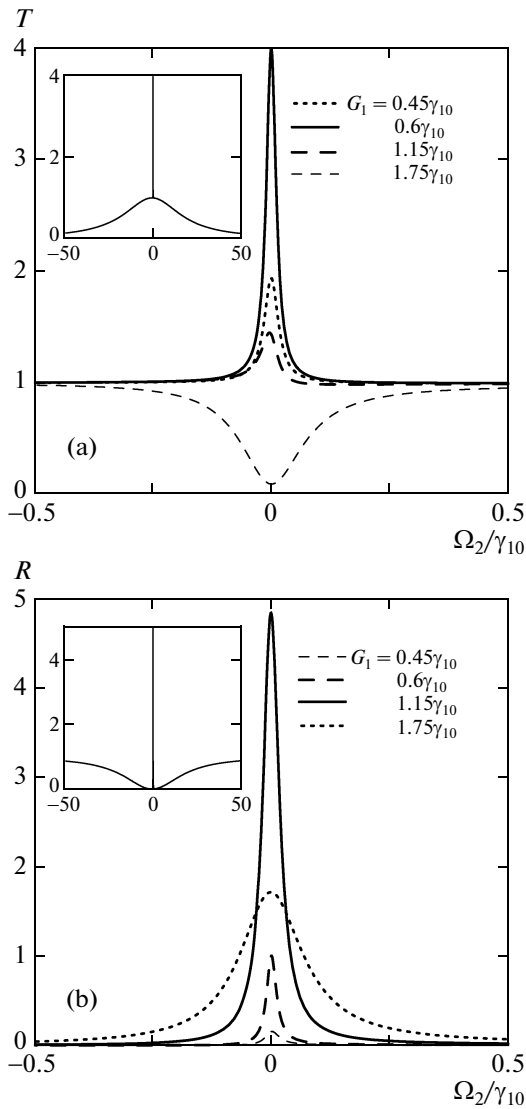


**Fig. 8.** (a) Transmission and (b) reflection spectra of the photonic crystal for various intensities of the control field for the case shown in Fig. 3b for  $\gamma_{10}/\gamma_{20} = 20$ .

Here,  $T_M$  and  $R_M$  are the transmittance and reflectance of the mirrors, respectively;  $\alpha = -(4\pi/\lambda)n''_{\text{eff}} > 0$  is the Raman gain factor of the probe wave; and  $\Phi = (4\pi/\lambda)n'_{\text{eff}}d$  is the phase delay in the double pass through the cavity, where  $n''_{\text{eff}} = 2\pi N\chi''_R F|E_{10}|^2$  and  $n'_{\text{eff}} = 1 + 2\pi N\chi'_R F|E_{10}|^2$  are the effective imaginary and real parts of the refractive index  $n_2$ , respectively;  $F$  is the spatial overlap integral of the pump and probe waves (details of the calculation of the effective refractive index and overlap integral are presented in the Appendix, see Eq. (A.2)); and  $E_{10}$  is the pump field amplitude in the Fabry–Perot cavity.

The condition  $\Phi = 2\pi m$  ( $m = 1, 2, \dots$ ) determines the resonance frequency of the cavity at which the transmittance is maximal,

$$T_{\max} = \frac{T_M^2 e^{\alpha d}}{(1 - R_M e^{\alpha d})}. \quad (7)$$

If  $\alpha d \ll 1$ , Eq. (7) can be represented in the form

$$T_{\max} \approx \frac{T_M^2}{(T_M - \alpha d R_M)^2}. \quad (8)$$

According to Eq. (8), under the condition  $\alpha d R_M < T_M$  and with an increase in the pump intensity,  $T_M - \alpha d R_M \rightarrow 0$ , the transmittance increases and can satisfy the condition  $T_{\max} \gg 1$ . In the opposite case where  $\alpha d R_M > T_M$ , as the pump field increases,  $T_{\max} \rightarrow 0$  in the Raman resonance region (see Figs. 4, 5); i.e., a dip appears in the transmittance. The condition  $R_M \exp(\alpha d) = 1$  is known as the threshold condition of the Raman laser. The reflectance can be analyzed similarly.

The FWHM of the narrow transmission peak is given by the expression

$$\delta\omega = \frac{\Delta\omega}{1 + \eta},$$

$$\Delta\omega = \frac{c |1 - R_M e^{\alpha d}|}{d e^{\alpha d/2} \sqrt{R_M}} \approx \frac{c |T_M - \alpha d R_M|}{d \sqrt{R_M}}.$$

Here,

$$\eta = 2\pi N F |E_{10}|^2 \omega_0 \frac{\partial \chi'_R}{\partial \omega_2} = \frac{F K_{12} |G_1|^2}{\Omega_1^2 \gamma_{20}^2},$$

where  $\omega_0$  is the resonance frequency of the empty cavity ( $n_D = 1$ ). The frequency derivative is taken at the point  $\omega_2 = \omega_0$ .

The formula for  $\Delta\omega$  at  $\alpha = 0$  is transformed to the known expression for the transmission width of the empty Fabry–Perot cavity [34],

$$\Delta\omega = c(1 - R_M)/d\sqrt{R_M}.$$

Note that  $1 + \eta$  at  $F = 1$  is equal to the index of the group velocity  $N_g = c/v_g$  for the probe wave in the presence of the Raman interaction (see Eq. (4)); this index can be much larger than unity when dispersion is large. Thus, the spectral width of narrow resonances of the probe Stokes field is inverse proportional to the index of the group velocity; i.e., the spectral width of this resonance decreases with a decrease in the group velocity.

Under the conditions  $\alpha d R_M < T_M$  and  $\eta \gg 1$ , the width of the transmission peak is by a factor of  $\eta$  smaller than that for the empty cavity; i.e., a narrow resonance appears in the transmission spectrum. The  $\eta$  value is determined by the dispersion of the Raman susceptibility and depends on the pump intensity. Analysis shows that the width of the resonance can be smaller than the width of the Raman transition  $\gamma_{20}$ . Note that when  $\alpha d R_M > T_M$ , the peak in the transmis-

sion spectrum changes to a dip according to Fig. 4, there is a narrow peak in the reflection spectrum, and the reflectance can be larger than unity ( $R > 1$ ). The intensity necessary for observing the effects under consideration depends on several parameters (the one-photon detuning of the pump frequency, the width of the Raman resonance, and the number of bilayers  $M$ ) and is estimated from several microwatts per square centimeter to several tens of milliwatts per square centimeter.

#### 4. CONCLUSIONS

The propagation of light through a photonic crystal cavity under the Raman gain conditions has been theoretically investigated. It has been shown that narrow and ultranarrow resonances can appear simultaneously in the transmission and reflection spectra of the probe (Raman) radiation. The spectral positions of these peaks are determined by the Raman resonance. The nature of narrow resonances is attributed to the dispersion of a nonlinear refractive index near the Raman transition; this dispersion is responsible for a strong decrease in the group velocity of the probe radiation. Narrowband lasers should be used to observe the considered effects. The combination of the Raman gain and photonic crystal cavities can be useful in various applications such as spectroscopy, atomic clock, quantum memory, and delay lines. We believe that, similar to EIT in an optical cavity [35, 36], the Raman gain can be also observed on cold atoms placed in photonic crystal structures, in particular on single atoms.

#### APPENDIX

##### EFFECTIVE REFRACTIVE INDEX IN THE FABRY–PEROT CAVITY

The field in the Fabry–Perot cavity has the form of standing waves, i.e., is inhomogeneous along the  $z$  axis. For this reason, we introduce the effective complex refractive index (averaged over the  $z$  axis) on the basis of the following simple consideration. The field in the cavity is represented in the form of the expansion in the eigenmodes of the empty cavity  $\sin(k_n z)$  ( $n = 1, 2$ ) [37]:

$$E_1 = E_{10} \sin(k_1 z), \quad E_2 = E_{20} \sin(k_2 z).$$

Here,  $k_1 = m\pi/d$  and  $k_2 = p\pi/d$ , where  $m$  and  $p$  are integers.

Since the polarization is a dipole moment per unit volume, the polarization at the probe field frequency can be represented in the form

$$P_R(\omega_2) = d^{-1} N \int_0^d \chi_R(\omega_2) |E_{10}|^2 E_{20} \sin^2(k_1 z) \sin(k_2 z) dz,$$

where the susceptibility  $\chi_R(\omega_2)$  is given by Eq. (1). From this relation, the effective susceptibility is expressed as

$$\chi_{R,\text{eff}}(\omega_2) = \frac{\chi_R(\omega_2)}{d} \int_0^d \sin^2(k_1 z) \sin(k_2 z) dz. \quad (\text{A.1})$$

The quantity

$$F = d^{-1} \int_0^d \sin^2(k_1 z) \sin(k_2 z) dz$$

can be treated as the overlap integral of the interacting waves. Using the standard procedure, the complex refractive index for the probe field is expressed from Eq. (A.1) as

$$\begin{aligned} n_{\text{eff}}(\omega_2) &= n'_{\text{eff}} + i n''_{\text{eff}} \\ &= \sqrt{1 + 4\pi N \chi_{R,\text{eff}}(\omega_2) |E_{10}|^2} \\ &\approx 1 + 2\pi N \chi_{R,\text{eff}}(\omega_2) |E_{10}|^2. \end{aligned} \quad (\text{A.2})$$

#### ACKNOWLEDGMENTS

This work was supported by the Council of the President of the Russian Federation for Support of Young Scientists and Leading Scientific Schools (project no. NSh-7810.2010.3), the Presidium of the Russian Academy of Sciences (project no. 27.1), the Ministry of Education and Science of the Russian Federation (state contract no. 02.740.11.0220), and the Siberian Branch, Russian Academy of Sciences (integration project no. 5).

#### REFERENCES

1. V. F. Shabanov, S. Ya. Vetrov, and A. V. Shabanov, *Optics of Real Photonic Crystals: Liquid-Crystal Defects and Inhomogeneities* (Siberian Branch of the Russian Academy of Sciences, Novosibirsk, 2005) [in Russian].
2. K. Busch, G. von Freymann, S. Linden, S. F. Mingaleev, L. Tkeshelashvili, and M. Wegener, Phys. Rep. **444**, 101 (2007).
3. J. Bravo-Abad, A. Rodrigues, P. Bermei, S. G. Johnson, J. D. Joannopoulos, and M. Soljacic, Opt. Express **15**, 16161 (2007).
4. P. Lalanne, C. Sauvan, and J. P. Hugonin, Laser Photonics Rev. **2**, 514 (2008).
5. K. J. Vahala, Nature (London) **424**, 839 (2003).
6. S. L. McCall, A. F. Levi, R. E. Slusher, S. J. Pearton, and R. A. Logan, Appl. Phys. Lett. **60**, 289 (1992).
7. D. W. Vernooy, A. Fugusawa, N. Ph. Georgiades, V. S. Ilchenko, and H. J. Kimble, Phys. Rev. A: At., Mol., Opt. Phys. **57** (4), R2293 (4 pages) (1998).
8. D. Englund, Y. Altug, B. Ellis, and J. Vučković, Laser Photonics Rev. **2**, 264 (2008).
9. X. Yang and C. W. Wong, Opt. Express **15**, 4723 (2007).
10. J. F. McMillan, X. Yang, N. C. Panoiu, R. M. Osgood, and C. W. Wong, Opt. Lett. **31**, 1235 (2006).
11. T. Baba, Nat. Photonics **2**, 465 (2008).
12. S. V. Spillane, T. J. Kippenberg, and K. J. Vahala, Nature (London) **415**, 621 (2002).

13. T. J. Kippenbregt, S. V. Spillane, D. K. Armani, and K. J. Vahala, Opt. Lett. **29**, 1224 (2004).
14. E. L. Ivchenko, M. A. Kaliteevski, A. V. Kavokin, and A. I. Nesvizhskii, J. Opt. Soc. Am. B **13**, 1061 (1996).
15. G. Khitrova and H. M. Gibbs, Rev. Mod. Phys. **71**, 1591 (1999).
16. S. John and V. Florescu, J. Opt. A: Pure Appl. Opt. **3**, S101 (2001).
17. V. G. Arkhipkin, S. A. Myslivets, I. V. Timofeev, A. V. Shabanov, S. Ya. Vetrov, and V. P. Timofeev, in *Proceedings of the Eighth International Conference on Laser and Fiber-Optical Networks Modeling (LFNM'2006), Kharkov, Ukraine, June 19–July 1, 2006* (Kharkov, 2006), p. 313.
18. M. Fleischhauer, A. Imamoglu, and J. P. Marangos, Rev. Mod. Phys. **77**, 633 (2005).
19. M. Soljacic and J. D. Joannopoulos, Nat. Mater. **3**, 211 (2004).
20. M. Soljacic, E. Lidorikis, L. V. Hau, and J. D. Joannopoulos, Phys. Rev. E: Stat., Nonlinear, Soft Matter Phys. **71**, 026602 (2005).
21. V. G. Arkhipkin and S. A. Myslivets, Kvantovaya Elektron. (Moscow) **39**, 157 (2009) [Quantum Electron. **39**, 157 (2009)].
22. M. G. Payne and L. Deng, Phys. Rev. A: At., Mol., Opt. Phys. **64**, 031 802 (2001).
23. S. Inouye, R. F. Löw, S. Gupta, T. Pfau, A. Görlitz, T. L. Gustavson, D. E. Pritchard, and W. Ketterle, Phys. Rev. Lett. **85**, 4225 (2000).
24. K. Lee and N. M. Lawandy, Appl. Phys. Lett. **78**, 703 (2001).
25. J. E. Sharping, Y. Okawachi, and A. L. Gaeta, Opt. Express **13**, 6092 (2005).
26. S. A. Akhmanov and N. I. Koroteev, *Methods of Nonlinear Optics in Light Scattering Spectroscopy* (Nauka, Moscow, 1981) [in Russian].
27. K. S. Repasky, L. Meng, J. K. Brasseur, J. L. Carlsten, and R. C. Swanson, J. Opt. Soc. Am. B **16**, 717 (1999).
28. M. Poecker and P. Kumar, Opt. Lett. **17**, 399 (1992).
29. D. N. Klyshko, *Physical Foundations of Quantum Electronics* (Nauka, Moscow, 1986; World Scientific, Singapore, 2010).
30. A. Yariv, *Quantum Electronics* (Wiley, New York, 1975; Sovetskoe Radio, Moscow, 1980).
31. R. W. Boyd, *Nonlinear Optics* (Academic, London, 1992).
32. A. Yariv and P. Yeh, *Optical Waves in Crystals: Propagation and Control of Laser Radiation* (Wiley, New York, 1984; Mir, Moscow, 1987).
33. A. V. Balakin, V. A. Bushuev, B. I. Mantsyzov, I. A. Ozheredov, E. V. Petrov, A. P. Shkurinov, P. Masselin, and G. Mouret, Phys. Rev. E: Stat., Nonlinear, Soft Matter Phys. **63**, 046609 (2001).
34. A. Yariv, *Introduction to Optical Electronics* (Holt, Rinehart, and Winston, New York, 1977; Vysshaya Shkola, Moscow, 1983).
35. Y. Shimizu, N. Shiokawa, N. Tamamamoto, M. Kozuma, T. Kuga, L. Deng, and E. W. Hagley, Phys. Rev. Lett. **89**, 233001 (2002).
36. J. Zhang, G. Hernandez, and Y. Zhu, Opt. Lett. **33**, 46 (2008).
37. S. Stenholm, *Foundations of Laser Spectroscopy* (Wiley, New York, 1984; Mir, Moscow, 1987).

*Translated by R. Tyapaev*